Electron paramagnetic resonance of Fe^{3+} in $LiNbO_3$

D. J. Keeble and M. Loyo-Menoyo
Carnegie Laboratory of Physics, Faculty of Engineering and Physical Sciences, University of Dundee, Dundee DD1 4HN, United Kingdom

Y. Furukawa
Oxide Corporation, Kobuchisawa, Yamanashi 408-004, Japan

K. Kitamura
National Institute for Materials Science, Tsukuba 305-0044, Japan

(Received 1 September 2004; revised manuscript received 7 March 2005; published 24 June 2005)

We report electron paramagnetic resonance (EPR) experiments on the dominant Fe^{3+} center in high-quality near stoichiometric $LiNbO_3$ grown from a Li/Nb ratio controlled melt. Symmetry related line splittings were clearly resolved and allowed unambiguous determination of the relative signs and magnitudes of the fourth-order trigonal zero field splitting (ZFS) spin-Hamiltonian (SH) parameters. Two conflicting EPR C_3 symmetry SHs for this center have been previously reported. Approximate agreement was found with that obtained for near-stoichiometric $LiNbO_3$ grown using a K_2O flux [G. I. Malovichko *et al.*, J. Phys.: Condens. Matter **5**, 3971 (1993)]. Extensive superposition model calculations of ZFS-SH terms showed that small displacement from either the Li or the Nb host site allowed the experimental rank-2 parameter value to be reproduced. Hence, on the basis of the EPR ZFS values alone, it is not currently possible to distinguish between possible C_3 incorporation sites within either the Li or Nb octahedra.

DOI: 10.1103/PhysRevB.71.224111 PACS number(s): 76.30.Fc, 77.84.Dy, 42.70.Mp, 61.72.Hh

I. INTRODUCTION

Lithium niobate is ferroelectric at room temperature and has a single phase transition to a paraelectric phase at 1473 K, approximately 57 K below the melting temperature. It has attracted sustained scientific and technical interest, mainly due to its desirable nonlinear optical properties. Doping with transition metal and rare-earth elements can enhance electrooptic coefficients and the photorefractive properties.[1,2] Photorefractive materials are used for holographic data storage and promise high storage densities with short access times. Significant advances have recently been made toward overcoming problems of sensitivity and volatile readout using near-stoichiometric $LiNbO_3$ codoped with Tb and Fe.[3] This work has refocused interest on the properties of Fe^{3+} in $LiNbO_3$.[4] Several methods capable of giving insight into the local site of incorporation including magnetic resonance techniques, Mössbauer spectroscopy, and extended x-ray absorption fine structure (EXAFS) have been applied. The latter, along with electron nuclear double resonance (ENDOR) experiments, have provided good evidence for Fe^{3+} incorporation at the Li site.[5–7] However, some electron paramagnetic resonance (EPR) experiments have been interpreted as providing evidence for Nb-site incorporation.[8–11] Further, the reported values for the fourth-order trigonal spin-Hamiltonian (SH) parameters obtained from EPR of Fe^{3+} in $LiNbO_3$ are not consistent.[9,12,13] The work presented here provides accurate values for these parameters and evaluates the application of the superposition model (SPM) analysis of the EPR parameters used to infer incorporation site information.

Electron paramagnetic resonance can readily detect Fe^{3+} ions, the main features of the spectra can be analyzed in terms of a spin-Hamiltonian of the form

$$\hat{\mathbf{H}} = \beta_e \mathbf{B}\cdot\mathbf{g}\cdot\hat{\mathbf{S}} + \sum_{k=2,4}\sum_{q=-k}^{k} f_k b_k^q \hat{\mathbf{O}}_k^q(S_x,S_y,S_z) \qquad (1)$$

containing electronic Zeeman and zero field splitting (ZFS) terms expressed using Stevens spin operators, the scaling factors relevant here take the values $f_2=1/3$ and $f_4=1/60$ and the explicit form of the spin operators are listed elsewhere.[14] The spin and site symmetry of the paramagnetic center dictate which terms are nonzero. For $S=\frac{5}{2}$ centers only terms $k=2,4$, with $-k\leqslant q\leqslant k$, are allowed.[15] The Laue class of the center point group imposes further constraints.[16] The two trigonal classes are relevant for the discussion of previous EPR studies, both allow nonzero ZFS terms b_2^0, b_4^0, b_4^{-3}, and b_4^3. By appropriate choice of the experimental xy axes either of the two fourth-order trigonal terms b_4^{-3} and b_4^3 can be set to zero since $[b_k^q]=\sin(q\phi)\{b_k^{-q}\}+\cos(q\phi)\{b_k^q\}$, where ϕ is a rotation of the xy axes about the C_3 axis.

In the ferroelectric phase $LiNbO_3$ is described by the $R3c$ space group, the crystal structure has been extensively studied,[17–21] a summary of relevant details is given in Table I. It is normally referred to a hexagonal unit cell containing six formula units and can be viewed as a sequence of distorted octahedra joined by their faces along a trigonal, polar, c axis. These are filled in the sequence Li, Nb, structural vacancy. The pairs of similar C_3 sites are related by $c/2$ glide operations, see Fig. 1. The standard orientation of the x, y, and z principal axes used to describe the physical properties of $LiNbO_3$ defines the z axis parallel to the hexagonal c axis and the x axis perpendicular to the glide plane so is parallel to a hexagonal a axis.[22] In this convention the glide plane is the zy plane. The point group for the octahedral sites is re-

TABLE I. Structural parameters for Li and Nb sites in $LiNbO_3$. Data from Inorganic Crystal Structure Database (ICSD). Polar coordinates with respect to conventional Cartesian axes. Azimuthally angle to first upper triangle oxygen ϕ_1, ϕ_2 similarly for the lower triangle. CG: congruent, NS: near stoichiometric.

Reference	17	18	18	19	20	20	21
ICSD code	28294	61118	61119	74469	80631	80632	85427
Crystal	CG	NS	CG		NS	CG	NS
Li/(Li+Nb)			0.482		0.498(2)	0.485(2)	0.492
c (nm)	1.38631(4)	1.385614(9)	1.386496(3)	1.38653	1.38581(4)	13.8647(4)	1.38495(2)
a (pm)	514.829(2)	514.739(8)	515.052(6)	515.02	514.85(1)	514.99(1)	514.44(1)
2α (Li site)	7.66°	7.41°	7.47°	7.51°	7.37°	7.52°	7.44°
R_1 (Li—O) (pm)	223.9	227.1	227.4	225.6	225.8	225.4	225.9
θ_1 (Li—O)	44.52°	43.97°	43.94°	44.32°	44.44°	44.37°	44.15°
ϕ_1	53.82°	53.90°	53.80°	53.80°	53.81°	53.80°	53.95°
R_2 (Li—O) (pm)	206.8	205.0	205.3	206.1	205.8	206.1	205.3
θ_2 (Li—O)	110.21°	109.22°	109.15°	109.76°	109.81°	109.83°	109.57°
ϕ_2	1.48°	1.31°	1.27°	1.32°	1.18°	1.32°	1.39°
2α (Nb site)	1.40°	1.24°	1.20°	1.23°	1.12°	1.23°	1.32°
R_1 (Nb—O) (pm)	188.9	187.6	187.9	184.3	187.2	187.9	187.8
θ_1 (Nb—O)	61.65°	62.10°	61.89°	64.09°	62.06°	61.92°	62.12°
ϕ_1	112.42°	112.65°	112.59°	142.57°	112.70°	112.57°	112.63°
R_2 (Nb—O) (pm)	211.2	213.0	212.6	218.0	213.3	212.6	212.6
θ_2 (Nb—O)	132.01°	132.24°	132.10°	133.66°	132.18°	132.14°	132.27°
ϕ_2	53.82°	53.89°	53.80°	53.82°	53.81°	53.80°	53.95°

duced from C_{3v} to C_3 by the slight twisting of the two trigonal oxygen atom planes with respect to each other. This is clearly seen in Fig. 1 and is quantified in Table I by the angle α. Large, high quality, $LiNbO_3$ crystals have normally been obtained from a congruently melting composition at about 48.5 mole % of Li_2O (51.5 mole % of Nb_2O_5).[23] Near stoichiometric material has been obtained by post-growth LiO_2 in-diffusion,[24] crystal growth using the addition of K_2O,[25] and by control of melt composition using a double crucible Czochralski method.[26]

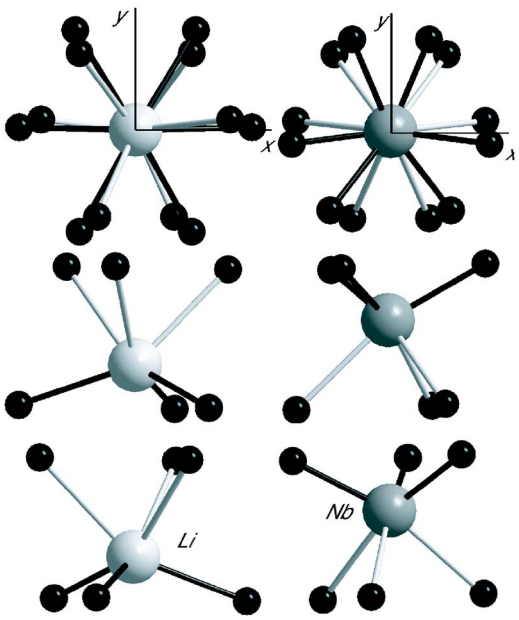

FIG. 1. Comparison of symmetry related Li and Nb sites (middle and bottom). Projection on the xy plane (top).

In the $LiNbO_3$ structure sites in one formula unit are related to equivalent sites in the other by the axial glide operation, see Fig. 1, the reflection operation, however, results in the nonequivalence of the SHs for the centers in the two sets of sites. The parameter transformations g_{xy} to $-g_{yx}$ and b_4^3 to $-b_4^3$ occur.[27] It is not possible to define ϕ as zero along either the x or y axes, due to the finite value of α. In consequence certain transitions observed as singlets in the glide plane, the zy plane, are expected to split into doublets in the zx plane, evidence of this behavior was presented by Malovichko *et al.*[12,28] The relevant EPR SHs from previous studies are given in Table II.

II. EXPERIMENTAL METHOD

Two near stoichiometric $3\times3\times8$ mm^3 crystals were studied, an x cut (major axis along [100]) and a z cut (major axis [001]) sample. The x axis is defined to be perpendicular to a glide plane. The x-cut sample was subsequently divided to allow the zx plane to also be studied. The samples were grown using a double crucible Czochralski method in which the growing crystal is in equilibrium with a Li-rich melt of 59 mol % Li_2O and 41 mol % Nb_2O_5.[26] The Curie temperature has been found to be sensitive to composition, this was measured by differential thermal analysis to be 1473 K, consistent with a nonstoichiometry $[Li_2O]/([Li_2O]+[Nb_2O_5])$ of 49.8%. The samples used in this study were not intentionally doped. EPR measurements were performed in the region

TABLE II. Spin-Hamiltonian parameters reported to C_3 symmetry for $b_2^0/h=5$ GHz Fe^{3+} center in $LiNbO_3$. The x-axis is defined to be perpendicular to the glide plane. CG: congruent, NS: near stoichiometric.

$g_\parallel$	$g_\perp$	b_2^0/h (GHz)	b_4^0/h (GHz)	$\lvert b_4^3\rvert/h$ (GHz)	b_4^{-3}/h (GHz)	$\lvert v_4^3\rvert/h$ (GHz)	Crystals	T (K)	Ref.
2.019	1.983	5.30(6)	−0.147(15)	1.95(15)	−1.14(15)	2.3	NS, K: 0.022 wt. %, reduced	25	12
1.984(3)	1.992(3)	4.917(15)	−0.162(18)	6.06(11)	0.27(4)	6.1	CG, Fe: 0.01 wt. %	~300	9
2.018(7)	1.999(7)	5.05(2)	−0.078(12)	0.7(6)	−2.16(8)	2.3	MgO: 5 mol % Fe: 0.05 mol %	~300	13

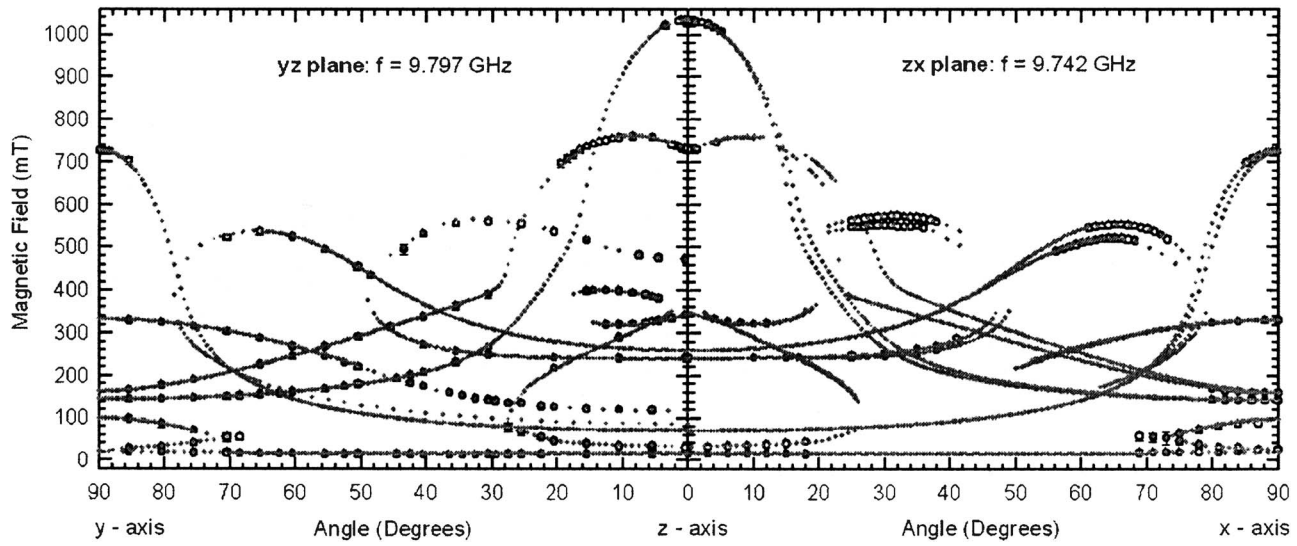

FIG. 2. Experimental EPR line positions (black open circles) and line positions simulated using spin-Hamiltonian parameters given in Table III (grey solid circles).

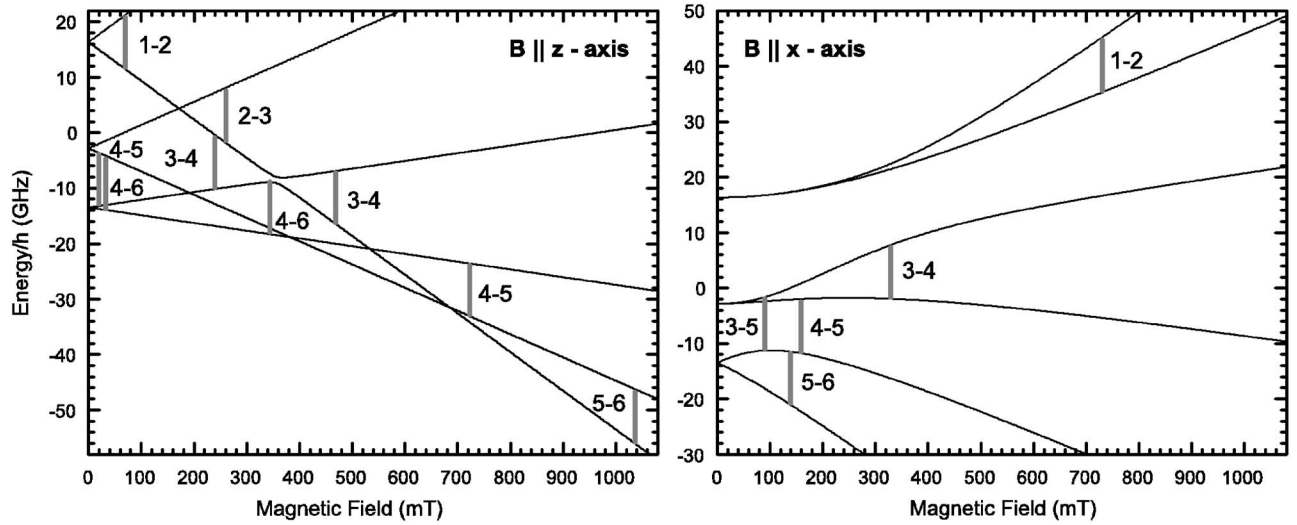

FIG. 3. Energy level diagrams for magnetic field parallel to z and x axes with observed EPR transitions marked.

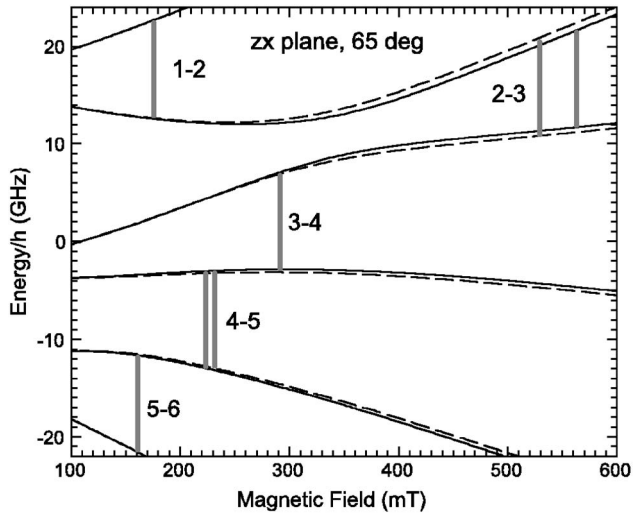

FIG. 4. Energy level diagram for the magnetic field direction of 65° in the *zx* plane. Levels calculated with $+b_4^3$ (solid line) and $-b_4^3$ (dashed line) shown along with EPR transitions.

of 9.5 GHz using a Bruker EMX spectrometer with a super-high-Q cavity and a matched low noise microwave bridge. The microwave frequency was measured using an EIP frequency counter. Measurements were made using two magnet systems, one with a maximum field B_{max} of 0.9 T, the other with B_{max}=2.1 T. The magnetic field was monitored on the 0.9 T system using an NMR magnetometer. The samples were mounted on an automated goniometer, which had an angular precision of ±0.125°. Variable temperature measurements were taken using an Oxford Instruments ESR900 cryostat. EPR spectral simulations were performed by exact diagonalization of the appropriate spin-Hamiltonian using the computer program EPR-NMR.[29]

III. EPR RESULTS

The room temperature EPR line positions measurements in both the *zy* and *zx* planes, due to the Fe^{3+} center, are shown in Fig. 2. In addition, transitions due to Mn^{2+} and Cr^{3+} centers were identified but are not shown. Detailed measurements where performed across the *zy* plane, in the *zx* plane measurements were focused mainly on those regions where doublets were observed. The energy level diagrams for the magnetic field directions parallel to the *z* and *x* axes are shown in Fig. 3, the observed EPR transitions marked. A similar diagram is shown in Fig. 4 for an angle of 65° in the *zx* plane. Two sets of levels result from the two inequivalent sites with sign reversed b_4^3 term values and results in splitting of several transitions in the plane perpendicular to the glide plane. An accurate magnitude for b_4^3 was determined fitting the simulated SH values for the 2-3 transitions for both the *zy* and *zx* planes, as well as the 3–5 transitions observed in region of 350 mT for the magnetic field parallel to the *z* axis. For b_4^{-3} again both 2-3 and 3–5 transitions were used. However, it should be noted that a number of transitions are sensitive to the fourth-order terms so an iterative process allowed accurate fit values to be obtained. The resulting SH parameters values are given in Table III and the line position shown in Fig. 2.

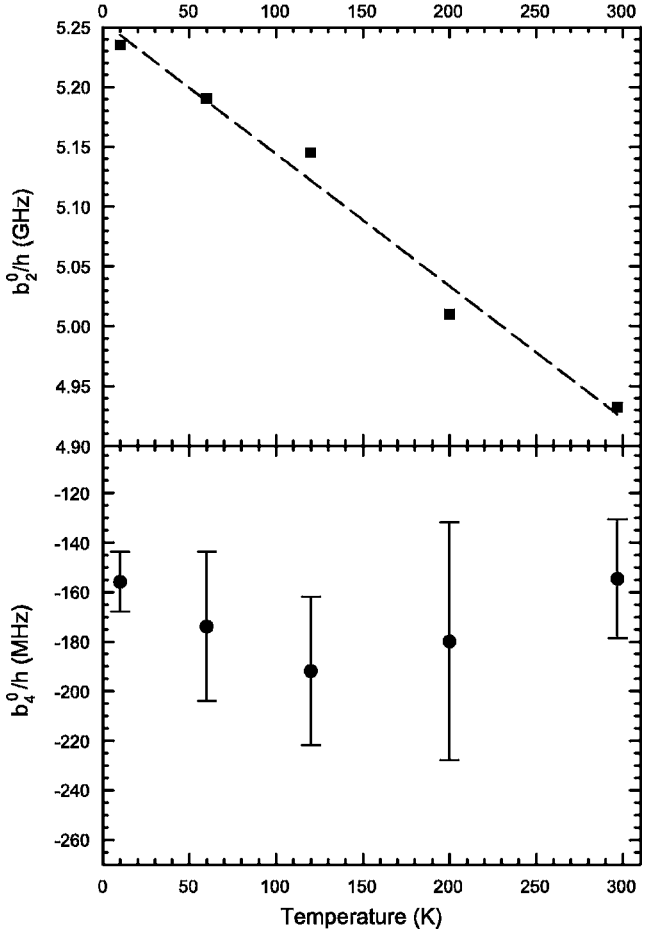

FIG. 5. Temperature dependence of ZFS parameters b_2^0 and b_4^0.

Comparison of line intensities for transitions 5-6 and 1-2 for B perpendicular to z were carried out between room temperature and 10 K and gave a positive sign for b_2^0. The temperature dependence of the SH parameters was determined through the range and the results are shown in Fig. 5. A linear behavior is observed for the rank 2 term $(b_2^0/h)(T) = (5.2543(2) - 0.0011(1)T)$ GHz. The temperature dependence of b_4^0 is also shown, the values of $|b_4^3|$ and b_4^{-3} were found to be constant within error.

TABLE III. Measured room temperature spin-Hamiltonian parameters for Fe^{3+} in $LiNbO_3$.

$g_\parallel$	$g_\perp$	b_2^0/h (GHz)	b_4^0/h (GHz)	$\lvert b_4^3\rvert/h$ (GHz)	b_4^{-3}/h (GHz)	$\lvert v_4^3\rvert/h$ (GHz)
1.996(3)	2.004(2)	+4.932(8)	−0.155(4)	3.5(2)	−0.84(1)	3.6

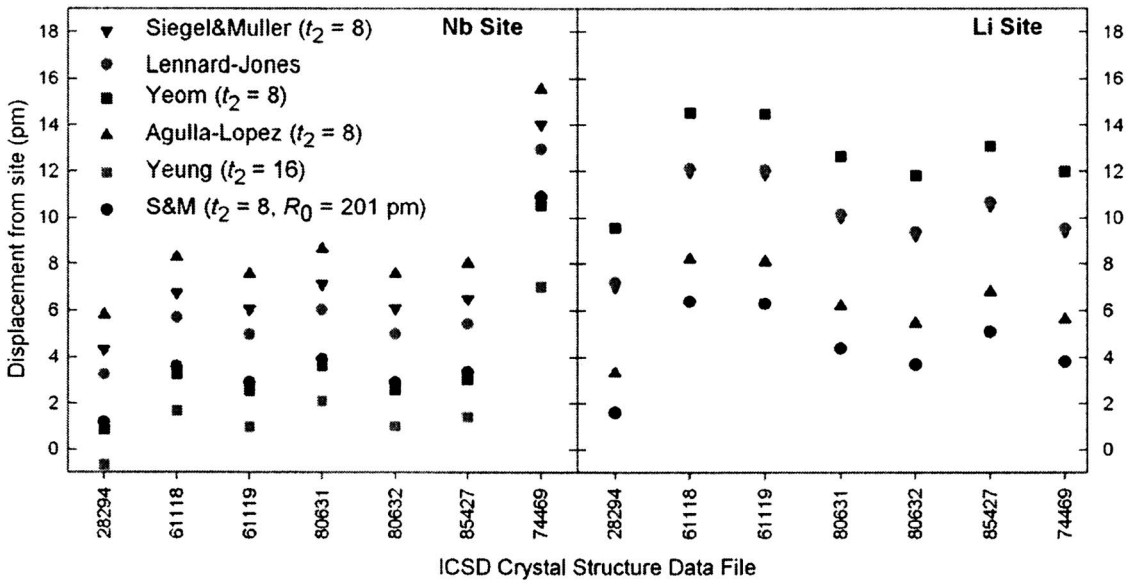

FIG. 6. Superposition model results for b_2^0 using the crystal structures detailed in Table I. The displacement from the host lattice site for which the calculated value is in agreement with experiment is shown. The methods of calculation are discussed in the text.

IV. SUPERPOSITION MODEL ANALYSIS

The Newman superposition model calculates ZFS terms using

$$b_k^q = \sum_L \bar{b}_k(R_L) K_{kq}(\theta_L, \phi_L), \tag{2}$$

where the intrinsic parameters $\bar{b}_k(R_L)$ represent the single paramagnetic ion-ligand pair contributions and $K_{kq}(\theta_L, \phi_L)$ are the appropriate angular functions.[30] The sum is over all nearest-neighbor ligands at angular positions (θ_L, ϕ_L) with respect to the paramagnetic ion. The intrinsic parameter can be expressed using the power-law (PL) approximation

$$\bar{b}_k(R) = \bar{b}_k(R_0)\left(\frac{R_0}{R}\right)^{t_k}, \tag{3}$$

or a Lennard-Jones (LJ)-type expression

$$\bar{b}_2(R) = -A\left(\frac{R_0}{R}\right)^n + B\left(\frac{R_0}{R}\right)^m. \tag{4}$$

The model parameter values $\bar{b}_k(R_0)$ or A and B are defined at a specific distance R_0, typically taken as the host site ion-ligand distance.[31,32]

TABLE IV. Superposition model parameter values for Fe^{3+} with O^{2-} ligands.

Host	R_0 (pm)	$\bar{b}_2/h$ (GHz)	t_2	Ref.	$\bar{b}_4/h$ (MHz)	Ref.
CaO	239.8	−6.75(60)	5(1)	34	27.3(1)	42
MgO	210.1	−12.35(75)	8(1)	34	87.8(1.4)	34
$SrTiO_3$	195.2	−20(3)	8(1)	34	84.9(1.4)	38
	200.0	−4.65(14)	16	35	29.7(2.4)	35

Calculations of b_2^0 were performed using several methods detailed by previous authors,[8,9,33–35] and using available $LiNbO_3$ crystal structures.[17–21] The distances from the Li and the Nb site positions to the nearest oxygen ligands are ~206 and 226 pm, and ~188 and 213 pm, respectively. These distances span the host ion-ligand distance for MgO. Calculations of b_2^0 were made assuming Fe^{3+} substituted at either the Li or the Nb site, and were performed for a series of displacements away from these sites. These were repeated for each of the crystal structure detailed in Table I. The values of Fe^{3+} displacement for which the SPM calculations were in agreement with the experimental result are shown in Fig. 6 for a representative selection of the calculations performed.

The conventional method of applying (2) for Fe^{3+} in octahedral coordination with oxygen is to use the intrinsic spin-Hamiltonian parameter $\bar{b}_2(R)$ defined by the PL expression (3) with the parameters given by Siegel and Müller and using the host ion-ligand separation as the reference distance R_0, see Table IV.[34] Yeom *et al.*,[9] modified this procedure by taking the Siegel and Müller MgO values but arbitrarily assign them, without a PL transformation, to new reference distances chosen to be the average of the ion-ligand separations, at either the Nb or Li site. Lennard-Jones calculations using (4) with $m=10$ and $n=13$ are also shown in Fig. 6, the parameter values were derived using the MgO PL parameters given in Table IV.

Two methods that attempt a quantitative correction to the SPM PL constants to account for charge misfit were also used. Agulló-López and Müller modify the magnitude of $\bar{b}_2(R_0)$ given for MgO in Table IV, based on the calculations of Sangster, it was increased by 22% when Fe^{3+} substitutes for Nb^{5+} and reduced by the same amount when substituted at the Li^+ site.[8,36] Yeung has also considered the effect of a local charge and size misfit.[35] The Siegel and Müller $\bar{b}_k$ values were used but were assigned to calculated R_0 values, for

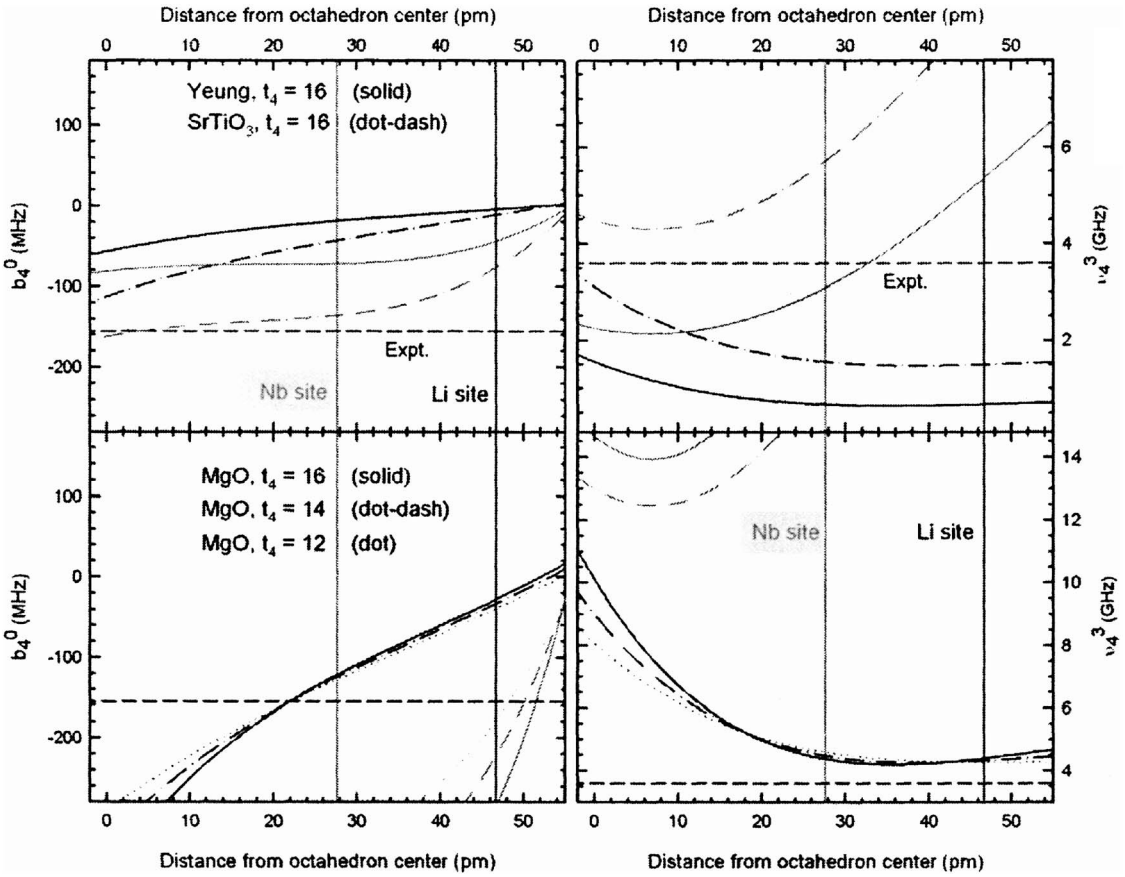

FIG. 7. Superposition model results for rank-4 SH terms using the crystal structure from Ref. 21. Displacements are from the center of the octahedron, the Nb and Li sites positions are marked. The methods of calculation are discussed in the text. The calculation result obtained using the Li octahedron are shown with black lines, those for the Nb octahedron in grey.

both $k=2$ and 4, and a consistent fit to PL expression was obtain, see Table IV.[35] The t_2 value of 16 is significantly higher than pervious values and result in displacements markedly different from the previous methods for the model of substitution for Li, these are not shown in Fig. 6 as they lie in the range -14 to -20 pm. Figure 6 also shows calculations performed using the conventional MgO intrinsic parameters but using the reference distance determined from EXAFS measurements.[37]

Fourth-order ZFS parameter calculations were also performed. The intrinsic parameter $\bar{b}_4$ is obtained directly from the fourth-order SH parameters for cubic host materials.[32] Newman and Siegel evaluate previous EPR studies of Fe^{3+} in the cubic hosts MgO and CaO and give values for $\bar{b}_4$ and estimates for the PL exponent t_4.[33] The values for $\bar{b}_4$ given by Newman and Siegel are commonly used and are reproduced in Table IV. The table also includes a $\bar{b}_4$ for Fe^{3+} in cubic $SrTiO_3$ obtained from a study by Müller.[38]

To directly determine a value for the PL exponent it is required that, in addition to the measurement of the fourth-order SH parameters, one or both of the relevant spin lattice parameters must be obtained from pressure-dependent measurements. Newman and Siegel used the second-order PL parameters for Fe^{3+} to estimate a t_4 value of 13.5, fitting experimental fourth-order SH parameters for $KNbO_3:Fe^{3+}$ gave a value of 12(4). Previously Walsh had obtained a t_4 value of 21.2 from hydrostatic pressure measurements of $MgO:Fe^{3+}$.[39] Mombourquette and Weil obtain a value for t_4 of 13(1) from a study of quasitetrahedrally bonded Fe^{3+} in quartz.[40] Yeung also considered fourth-order SPM calculations, see Table IV, and determined an approximate value for t_4 of 16(4).[35] Yeom *et al.* performed SPM calculations of the $LiNbO_3:Fe^{3+}$ fourth-order SH terms using $\bar{b}_4$ for MgO, as well as with value (57.3 MHz) obtained by averaging the MgO and CaO values.[9] The calculation method was similar to that used for b_2^0, the $\bar{b}_4$ was assigned to a reference distance chosen to be the average of the ion-ligand separations, at either the Nb or Li site.[9]

The calculations were made for Fe^{3+} substituted at, and displaced from, the Li and the Nb sites in the $LiNbO_3$ crystal structures shown in Table I. Figure 7 shows a representative set of calculations performed using the structure reported by Lehnert *et al.*[21] The variations observed between the structures given in Table I were found to be less than those obtained using the different SPM parameter sets given in Table IV. No calculations produced a simultaneous fit of the experimental fourth-order SH parameters b_4^0, $|b_4^3|$, and b_4^{-3}, for an accessible displacement from either site. Figure 7 compares calculated and experimental b_4^0 and v_4^3 values as a function of displacement from the center of the each octahedron.

V. DISCUSSION

The detailed roadmap of EPR line position obtained in both the *zx* and *zy* planes has allowed the spin-Hamiltonian parameters to fourth-order to be accurately determined. These confirm that the Fe^{3+} center site lies on the C_3 axis. The SH results presented in Table III and Fig. 5, show approximate agreement with those of Malovichko *et al.*,[12] but the fourth-order trigonal terms values are inconsistent with those reported with Yeom and co-workers.[9,13] The temperature dependence of the SH parameters determined here can be compared to that reported by Mehan and Scott,[41] the former work studied the dependence from 313 to 573 K and found $(b_2^0/h)(T)=(5.4495-0.0015T)$ GHz. A linear decrease with increasing temperature was also reported for b_4^0. While a linear decrease in b_2^0 was observed here for the temperature range 5 to 300 K, the gradient is less than that found in the high temperature study and the fourth order terms were found to be temperature independent, within experimental error. It would be of interest to study the ZFS term dependence in a near-stoichiometric crystal to higher temperatures. In fitting the experimental roadmap there is interplay between the two axial terms b_2^0 and b_4^0 which can lead to ambiguity in the value of the smaller parameter if the number of transitions is small or their linewidths are large.

To gain further insight on the location of the local structure the superposition model must be used. This allows the values of the ZFS terms to be calculated using the position of the nearest-neighbor ligand ions. The largest is the axial second order term b_2^0 the SPM calculations allow the observed value to be reproduced for plausible displacements from either the Li or Nb site toward the center of the relevant octahedron, see Fig. 6. Given the uncertainties in the SPM it is not possible to determine in which octahedron the center lies. The positions of the oxygen ions for the two octahedra are too similar.

Extension of the SPM calculations to the fourth rank ZFS terms was found to provide a severe test of the model. All three terms are obtained from the calculation and simultaneous agreement with the experimental values should be observed for a specific nearest-neighbor geometry. This geometry should also give the correct rank 2 term value. For the model examined of rigid oxygen octahedron, with Fe^{3+} ion displacements along the *z* axis, no such agreement was found. Figure 7 shows the variation in the calculated b_4^0 and magnitude term v_4^3 as a function of displacement. The failure of these fourth-order calculations may be due to inaccurate fourth-order model intrinsic parameter values or to the restriction of the calculations to unrelaxed oxygen octahedra, or to a combination of both.

The EPR ZFS terms are dominated by the configuration of the nearest-neighbor oxygen ions, experimental methods that provide information on near neighbor cations are expected to be less influenced by local relaxation. Both ENDOR and EXAFS experiments locate Fe^{3+} within the Li octahedron.[5–7]

VI. CONCLUSIONS

The significantly narrower Fe^{3+} EPR linewidths observed for near-stoichiometric $LiNbO_3$ crystals grown directly from a Li/Nb ratio controlled melt has allowed line splittings in the plane perpendicular to the glide plane to be clearly resolved. These splittings allowed an accurate unambiguous spin-Hamiltonian fit to be obtained with C_3 symmetry, see Table III, confirming that Fe^{3+} ions substitute at sites on the trigonal axis. The resulting SH is in approximate agreement with that reported by Malovichko *et al.*,[12] who studied near-stiochiometric crystals grown using a K_2O flux.

Extensive superposition model calculations of the second and fourth rank SH terms were performed and show that the local environments at the Li and Nb sites are too similar to be distinguished using the currently available model parameter values. Experimental methods that allow the nature of the neighbor cations to be determined should provide a more reliable assignment of the center to a specific C_3 symmetry site than can be currently achieved from analysis of the EPR zero field splitting terms.

ACKNOWLEDGMENTS

D.J.K. wishes to acknowledge support from Carnegie Research Grants for this work and M.L.M. was supported by EPSRC.

[1] Y. Kondo, K. Fukuda, Y. Yamashita, K. Yokoyama, K. Arita, M. Watanabe, Y. Furukawa, K. Kitamura, and H. Nakajima, Jpn. J. Appl. Phys., Part 1 **39**, 1477 (2000).

[2] D. L. Staebler and W. Phillips, Appl. Phys. Lett. **24**, 268 (1974).

[3] M. Lee, S. Takekawa, Y. Furukawa, K. Kitamura, and H. Hatano, Phys. Rev. Lett. **84**, 875 (2000).

[4] M. Lee, I. Gyoo Kim, S. Takekawa, Y. Furukawa, Y. Uchida, K. Kitamura, and H. Hatano, J. Appl. Phys. **89**, 5311 (2001).

[5] C. R. A. Catlow, A. V. Chadwick, M. Cole, and S. M. Tomlinson, Radiat. Eff. Defects Solids **119**, 565 (1991).

[6] T. S. Bush, C. R. A. Catlow, A. V. Chadwick, M. Cole, R. M. Geatches, G. N. Greaves, and S. M. Tomlinson, J. Mater. Chem. **2**, 309 (1992).

[7] H. Sothe and J. M. Spaeth, J. Phys.: Condens. Matter **4**, 9901 (1992).

[8] F. Agullo-Lopez and K. A. Muller, Cryst. Lattice Defects Amorphous Mater. **15**, 89 (1987).

[9] T. H. Yeom, Y. M. Chang, S. H. Choh, and C. Rudowicz, Phys. Status Solidi B **185**, 409 (1994).

[10] M. G. Zhao and M. Chiu, Phys. Rev. B **49**, 12 556 (1994).

[11] T. H. Yeom and S. H. Choh, J. Korean Phys. Soc. **32**, S672 (1998).

[12] G. I. Malovichko, V. G. Grachev, O. F. Schirmer, and B. Faust, J. Phys.: Condens. Matter **5**, 3971 (1993).

[13] T. H. Yeom, S. H. Lee, S. H. Choh, and D. Choi, J. Korean Phys. Soc. **32**, S647 (1998).

[14] A. Abragam and B. Bleaney, *Electron Paramagnetic Resonance of Transition Ions* (Clarendon Press, Oxford, 1970).
[15] V. G. Grachev, Zh. Eksp. Teor. Fiz. **92**, 1834 (1987).
[16] D. G. McGavin, J. Magn. Reson. (1969-1992) **74**, 19 (1987).
[17] S. C. Abrahams, J. M. Reddy, and J. L. Bernstein, J. Phys. Chem. Solids **27**, 997 (1966).
[18] S. C. Abrahams and P. Marsh, Acta Crystallogr., Sect. B: Struct. Sci. **42**, 61 (1986).
[19] M. Ohgaki, K. Tanaka, and F. Marumo, Mineral. J. **16**, 150 (1992).
[20] N. Iyi, K. Kitamura, F. Izumi, J. K. Yamamoto, T. Hayashi, H. Asano, and S. Kimura, J. Solid State Chem. **101**, 340 (1992).
[21] H. Lehnert, H. Boysen, F. Frey, A. Hewat, and P. Radaelli, Z. Kristallogr. **212**, 712 (1997).
[22] R. S. Weis and T. K. Gaylord, Appl. Phys. A **37**, 191 (1985).
[23] J. R. Carruthers, G. E. Peterson, M. Grasso, and P. M. Bridenbaugh, J. Appl. Phys. **42**, 1846 (1971).
[24] P. F. Bordui, R. G. Norwood, D. H. Jundt, and M. M. Fejer, J. Appl. Phys. **71**, 875 (1992).
[25] G. I. Malovichko, V. G. Grachev, L. P. Yurchenko, V. Y. Proshko, E. P. Kokanyan, and V. T. Gabrielyan, Phys. Status Solidi A **133**, K29 (1992).
[26] K. Kitamura, J. K. Yamamoto, N. Iyi, S. Kimura, and T. Hayashi, J. Cryst. Growth **116**, 327 (1992).
[27] G. I. Malovichko, V. G. Grachev, and S. N. Lukin, Fiz. Tverd. Tela (Leningrad) **28**, 991 (1986).
[28] Note that Figs. 2 and 3 in Ref. 11 are mislabeled. The axes convention is correctly described in the text.
[29] Computer Program EPR-NMR, Department of Chemistry, University of Saskatchewan, Canada.
[30] D. J. Newman and W. Urban, J. Phys. C **5**, 3101 (1972).
[31] K. A. Muller and W. Berlinger, J. Phys. C **16**, 6861 (1983).
[32] D. J. Newman and W. Urban, Adv. Phys. **24**, 793 (1975).
[33] D. J. Newman and E. Siegel, J. Phys. C **9**, 4285 (1976).
[34] E. Siegel and K. A. Muller, Phys. Rev. B **19**, 109 (1979).
[35] Y. Y. Yeung, J. Phys. C **21**, 2453 (1988).
[36] M. J. L. Sangster, J. Phys. C **14**, 2889 (1981).
[37] G. A. Waychunas, J. Mater. Sci. **18**, 195 (1983).
[38] K. A. Muller, Helv. Phys. Acta **31**, 173 (1958).
[39] W. M. Walsh, Jr., Phys. Rev. **122**, 762 (1961).
[40] M. J. Mombourquette, J. Minge, M. R. Hantehzadeh, J. A. Weil, and L. E. Halliburton, Phys. Rev. B **39**, 4004 (1989).
[41] F. Mehran and B. A. Scott, Solid State Commun. **11**, 15 (1972).
[42] A. J. Shuskus, Phys. Rev. **127**, 1529 (1962).